

RESEARCH ARTICLE

# 3D printing of drug-eluting bioactive multifunctional coatings for orthopedic applications

Eben Adarkwa<sup>1</sup>, Abhijit Roy<sup>2,3</sup>, John Ohodnicki<sup>2</sup>, Boeun Lee<sup>2</sup>, Prashant N. Kumta<sup>2,4,5</sup>, Salil Desai<sup>1\*</sup>

<sup>1</sup>Center of Excellence in Product Design and Advanced Manufacturing, North Carolina Agricultural and Technical State University, Greensboro, North Carolina, USA

<sup>2</sup>Department of Bioengineering, University of Pittsburgh, Pittsburgh, Pennsylvania, USA

<sup>3</sup>Kennametal Inc., Latrobe, Pennsylvania, USA

<sup>4</sup>Department of Chemical and Petroleum Engineering, University of Pittsburgh, Pittsburgh, Pennsylvania, USA

<sup>5</sup>Department of Mechanical Engineering and Materials Science, University of Pittsburgh, Pittsburgh, Pennsylvania, USA

(This article belongs to the *Special Issue: Additive Manufacturing of Functional Biomaterials*)

## Abstract

Three-dimensional (3D) printing is implemented for surface modification of titanium alloy substrates with multilayered biofunctional polymeric coatings. Poly(lactic-co-glycolic) acid (PLGA) and polycaprolactone (PCL) polymers were embedded with amorphous calcium phosphate (ACP) and vancomycin (VA) therapeutic agents to promote osseointegration and antibacterial activity, respectively. PCL coatings revealed a uniform deposition pattern of the ACP-laden formulation and enhanced cell adhesion on the titanium alloy substrates as compared to the PLGA coatings. Scanning electron microscopy and Fourier-transform infrared spectroscopy confirmed a nanocomposite structure of ACP particles showing strong binding with the polymers. Cell viability data showed comparable MC3T3 osteoblast proliferation on polymeric coatings as equivalent to positive controls. *In vitro* live/dead assessment indicated higher cell attachments for 10 layers (burst release of ACP) as compared to 20 layers (steady release) for PCL coatings. The PCL coatings loaded with the antibacterial drug VA displayed a tunable release kinetics profile based on the multilayered design and drug content of the coatings. Moreover, the concentration of active VA released from the coatings was above the minimum inhibitory concentration and minimum bactericidal concentration, demonstrating its effectiveness against *Staphylococcus aureus* bacterial strain. This research provides a basis for developing antibacterial biocompatible coatings to promote osseointegration of orthopedic implants.

**Keywords:** Antibacterial; 3D printing; Orthopedic implants; Osseointegration; Polymeric coatings; Therapeutic agents

**\*Corresponding author:**

Salil Desai  
(sdesai@ncat.edu)

**Citation:** Adarkwa E, Roy A, Ohodnicki J, *et al.*, 2023, 3D printing of drug-eluting bioactive multifunctional coatings for orthopedic applications. *Int J Bioprint*, 9(2): 661.  
<https://doi.org/10.18063/ijb.v9i2.661>

**Received:** July 02, 2022

**Accepted:** September 02, 2022

**Published Online:** January 04, 2023

**Copyright:** © 2023 Author(s). This is an Open Access article distributed under the terms of the Creative Commons Attribution License, permitting distribution, and reproduction in any medium, provided the original work is properly cited.

**Publisher's Note:** Whioce Publishing remains neutral with regard to jurisdictional claims in published maps and institutional affiliations.

## 1. Introduction

Tissue surface modification is implemented on a medical implant device to enhance its biocompatibility, wear resistance, corrosion resistance, performance, and therapeutic

effectiveness<sup>[1-3]</sup>. The careful choice and application of coating materials at the implant interface are key to its success. The incorporation of drugs or biofactors within polymeric encapsulation on metallic implants not only serves as a conduit for spatiotemporal bioagent<sup>[4-7]</sup> delivery but also provides surface modification properties to improve the biocompatibility and overall clinical performance of the implant device<sup>[8-10]</sup>.

Titanium and its alloys are widely used in orthopedic implants for the past several decades<sup>[11-13]</sup>. Despite sterilization and aseptic procedures, bacterial infections associated with titanium-based orthopedic implantation are still a major challenge and cause implant failure<sup>[14-21]</sup>. The main reason for implant surface vulnerability to infection is the formation of a surface biofilm, which compromises the immune capability at the implant/tissue interface<sup>[14,20-23]</sup>. At present, several methods are in place to prevent implant-associated bacterial infections. They involve incorporating antimicrobial agents into polymeric implant coatings, engineering polymeric coatings to actively release tunable antimicrobial agents, and finally, altering the surface physiochemical properties of the implant device<sup>[20,21,24-26]</sup>. Molecular mechanisms for drug and growth factor elution have been studied to enhance its adsorption behavior on a variety of substrates<sup>[27-31]</sup>. The effect of liquid-surface interactions impacting different applications has been widely studied using atomistic modeling<sup>[32-35]</sup>. According to Hetrick *et al.*<sup>[21]</sup>, delivering the antibiotic in a tunable manner at the implant site from a polymeric surface coating is the preferred approach to improving the efficacy of conventional antibiotics against implant-associated bacterial infection. Loading antibiotics into bioresorbable polymeric coatings have proven to be effective in eliminating or reducing bacterial infection associated with orthopedic implants<sup>[14,16,17,36-42]</sup>.

Different disposition techniques have been utilized for the coating of biomedical devices with each having their own respective advantages and disadvantages. Some of the prominent processes used in the bioprinting field include inkjet printing, stereolithography, laser-induced forward transfer, and extrusion deposition. Jiang *et al.*<sup>[43]</sup> discussed different types of extrusion heads and material compositions using pneumatic and mechanical actuation mechanisms. Similarly, Zhuang *et al.*<sup>[44]</sup> presented a facile bioprinting strategy that combines the rapid extrusion-based bioprinting technique with an in-built ultraviolet (UV) curing system to facilitate the layer-by-layer UV curing of bioprinted photocurable GelMA-based hydrogels. Li *et al.*<sup>[45]</sup> have outlined the use of inkjet printing for drug development, scaffold building, and cell depositing in their review article. They elucidate the concept of

biopixels which combine characteristics of inkjet printing and basic biological units. Ng *et al.* identified optimal droplet velocity and droplet volume to mitigate adverse impact on cell survivability and droplet splashing with sub-nanoliter-based bioprinting<sup>[46]</sup>. Vat polymerization (VP) is 3D printing process that uses UV light as a curing mechanism for a desired object in a prefilled vat. Several researchers<sup>[47]</sup> have conducted a comprehensive review of the materials, process conditions, regulatory challenges, and future directions in VP toward tissue engineering and regenerative medicine applications. Further, new VP strategies are discussed for *in vivo* regeneration and drug screening therapeutics including biomaterial ink formulations and VP system designs<sup>[47]</sup>. Thus, it is evident that a multitude of biofabrication processes are available based on the type of biomaterial and configuration of tissue construct to be manufactured for a specific application.

Our research group employs a customized 3D printing coating technique to uniformly deposit multilayers of polymeric formulations embedded with therapeutic agents<sup>[48-53]</sup>. In our previous work, basic inkjet printing was utilized for polyester urethane urea coatings embedded with paclitaxel (Taxol) agent for cardiovascular stent applications. Similarly, different polymeric coatings were evaluated for their corrosion protection potential on magnesium alloys for tracheal applications. Unlike, above-described simpler approaches, a retrofitted 3D printing system was utilized in this research which can deposit multilayered structures for 3D scaffolds and have *in situ* infiltration capability for specific growth factors, biomaterials and cell-laden media. Further, we synthesized a unique ink formulation which includes both bone promoting and antibacterial agents simultaneously. These include nanoparticulates of amorphous calcium phosphate (ACP) for promoting osseointegration and antibiotic (vancomycin [VA]) to eliminate bacterial infections in orthopedic implant applications. The implementation of multilayered coatings has proven to be effective in providing tunable release of different growth and healing agents when encapsulated within bioresorbable polymeric thin films<sup>[54-56]</sup>. In the field of polymer deposition, inkjet technology has several advantages<sup>[57]</sup> making it an ideal technique for coating implant devices. The problems associated with conventional polymer/drug loading coating techniques have been discussed extensively by de Gans *et al.*<sup>[57]</sup>. They range from the inability to vary drug distribution in a controlled manner for a specific drug loading profile, variations, and inconsistency in drug concentration from device to device, recurrent webbing between the struts, and the inability to control the local density of the drug. The use of the drop-on-demand inkjet printing eliminates issues associated with the conventional

coating techniques and offers numerous advantages as discussed by Cooley *et al.*<sup>[48]</sup> as, “Inkjet-based deposition requires no tooling, is non-contact, and is data driven; no masks or screens are required; the printing information is created directly from CAD information stored digitally. Being data driven, it is flexible. As an additive process with no chemical waste, it is environmentally friendly and cost effective.”

In this work, the custom 3D printing method was employed to achieve precision deposition of uniform multilayer coatings. The biofunctional coatings consisted of ACP and VA formulations mixed within a biodegradable polymeric matrix. VA is a glycopeptide antibiotic which is used to treat serious infections of many Gram-positive bacteria<sup>[58,59]</sup>. It was hypothesized that the steady release of antibiotics would eliminate the bacterial infection on the titanium implant surfaces, whereas the presence of ACP would aid in osseointegration and wound healing process.

## 2. Materials and methods

Nanoparticles of ACP were synthesized by controlled precipitation using water-soluble calcium and phosphate salts. Biodegradable poly(D, L-lactic-co-glycolic) acid (PLGA 50:50) and polycaprolactone (PCL Mn ~2,000) polymers were obtained from Sigma-Aldrich. 2,2,2-trifluoroethanol (TFE) obtained from Aldrich, St. Louis, MO, was used as a solvent for dissolution. VA (vancomycin hydrochloride, Alfa Aesar, USA) was used as a model antibiotic known for its efficacy in treating bacterial infections associated with orthopedic implants<sup>[15,16,18,60,61]</sup>. Mechanically polished thin titanium (Ti) alloy coupons (10 mm × 10 mm × 1 mm) were used as the substrates for depositing the embedded polymeric materials.

### 2.1. Substrate cleaning procedure

Titanium alloy coupons (substrates) underwent a cleaning procedure. The pre-cleaning treatment of Ti coupon substrates involved an initial rinsing of the coupon substrates with ethanol to remove organic surface impurities followed by further rinsing with distilled water. The rinsed Ti substrates were then dipped and washed in 3 mol L<sup>-1</sup> of nitric acid in water for degreasing. After that, the substrates were washed with excess deionized water to remove the acids at the surface and then were air-dried. In the mechanical polishing process, a 1200 grit size SiC paper was used to eliminate surface adhered impurities. Polishing was performed on both surfaces of the Ti substrates. The polished surfaces were then finally rinsed using deionized water and the samples were subsequently air-dried and stored in a Class 1000 cleanroom.

### 2.2. Coating solution preparation

Two types of printing solutions were formulated depending on the type of study or characterization to be performed. These include solutions of ACP only (polymer\_ACP only) within the polymer and a combination of both ACP and VA (polymer\_ACP\_VA) in the polymer solution. Different formulations of each type of coating “ink solution” were prepared by dissolving certain amounts of PLGA or PCL in TFE solvent and stirring for 2 h. The concentrations of both PLGA and PCL solutions were fixed at 1 wt. % polymer in the solvent. These biopolymer solutions were further blended with ACP at 0.5 – 1% w/v concentrations based on the coating to be evaluated (Table 1). The resultant polymer/ACP solution was mixed, stirred for 2 h, and further ultrasonicated for 4 h to obtain a completely homogeneous mixture. All printing solutions were filtered (30 μm – mesh) to remove large ACP and VA particulates to prevent them from clogging the printing nozzles. Titanium samples coated with this printing solution were used for materials characterizations and *in vitro* studies. Printing solutions consisting of VA were prepared from an initial 1 wt. % PCL in TFE solvent. The polymeric solution was further homogeneously blended with 1 – 2% w/v VA based on the coating to be evaluated (Table 2). Titanium alloy substrates coated with these printing solutions were used for antibiotic release measurements and antibiotic activity studies.

### 2.3. Printing procedure

A customized hybrid inkjet system was employed for this research. A printing nozzle with an orifice dimension of 50 μm was used for all the printing procedures. A motion controller printing script was coded for uniformly coating each Ti alloy substrate. The substrate temperature was controlled at 20°C. Uniform coatings of 10 or 20 layers were printed on the Ti substrates. Figure 1 shows the custom 3D printing equipment and schematic for depositing the

**Table 1. Experimental design and ink composition for *in vitro* cellular viability and cytocompatibility assessments**

Sample code	Polymer type	ACP concentration (% w/v)	No. of layers
1	PCL	0.5	20
2	PCL	0.5	10
3	PLGA	0.5	20
4	PLGA	0.5	10
5	PCL	1	20
6	PCL	1	10
7	PLGA	1	20
8	PLGA	1	10

**Table 2. Experimental design and ink composition for vancomycin release measurements and antimicrobial studies**

Sample code	Polymer type	Polymer concentration (%wt)	Vancomycin concentration (% w/v)	ACP concentration (% w/v)	No. of layers
R-1	PCL	1	1	0	20
R-2	PCL	1	2	0	10
R-3	PCL	1	2	1	20

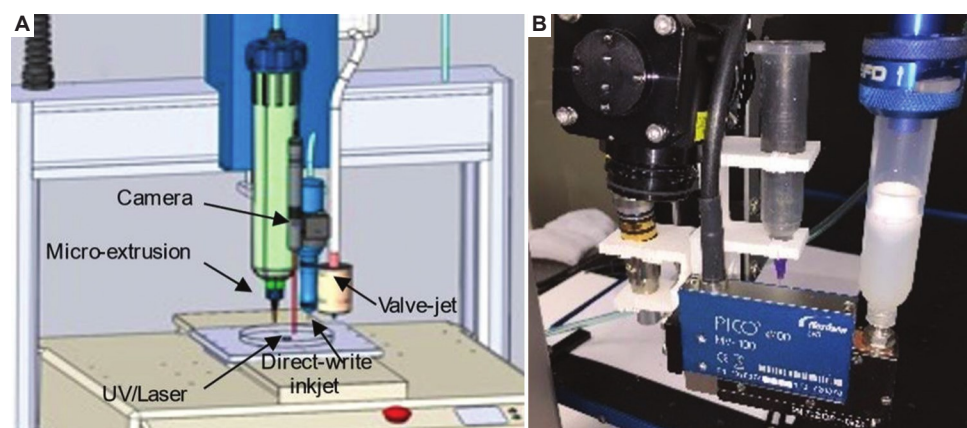


**Figure 1.** (A) Schematic of the custom 3D direct-write inkjet equipment. (B) Experimental setup for the deposition of composite polymeric formulations and *in situ* infiltration.

polymeric formulations on the Ti substrates. As compared to our earlier work, this system consists of a combination of deposition units including microextrusion, inkjet, and valve jet systems that can both deposit 3D tissue scaffolds and infiltrate biomedia at specific target locations. The UV/laser system enables curing of hydrogels and other photopolymers. In addition, camera system mounted on the unit can capture real-time deposition images for closed-loop feedback.

#### 2.4. Design of experiment

The experimental design and starting ink compositions to print the films for the osteoblast culture/assay and antibiotic release measurements characterization are shown in Tables 1 and 2, respectively. For osteoblast culture/assay studies, the coating thickness was varied by printing 10 and 20 layers of the films, and the ACP concentration was varied at 0.5% w/v and 1% w/v, whereas the polymeric solution was fixed at 1 wt. % polymer in solvent. The run sequence for the coating process was determined randomly and each experimental run was replicated 5 times ( $n = 5$ ) to enable the variability associated with the experimental units to be estimated. A total of 40 ( $n = 40$ ) samples were prepared for both characterization and *in vitro* studies. Two samples ( $n = 2$ ) from each experimental run were used for coating characterization studies (optical microscopy, scanning electron microscopy [SEM], and Fourier-transform infrared [FTIR] spectroscopy), whereas the

other three samples ( $n = 3$ ) were used for *in vitro* viability and cytocompatibility assessment. Bare Ti substrate and tissue culture polystyrene (TCPS) samples were used as positive controls.

The coating thickness for antibiotic release measurements and bacterial culture studies was varied at 10 and 20 layers, with the ACP concentration being varied between 0 and 1% w/v whereas VA was varied at 1 and 2% w/v concentrations, respectively. The polymeric solution was fixed at 1 wt.% polymer in TFE solvent. The run sequence for the coating process was determined randomly and each experimental run was replicated 5 times ( $n = 5$ ). Two samples ( $n = 2$ ) from each experimental run were used for coating characterization studies (SEM and FTIR) whereas the other three samples ( $n = 3$ ) were used for release kinetics and bacterial culture studies. Bare Ti alloy substrates used for printing were weighed before and after coating. Coated samples were kept in a 4°C refrigerator until release study was conducted.

#### 2.5. Coating characterization

The uniformity of the different coating samples fabricated was studied using the optical microscopy (Keyence VHX 600K Digital Microscope). The surface morphology of the coatings was studied using a scanning electron microscope (Philips-XL30 FEG, Philips) operating at 10.0 kV. The samples used for SEM analysis were coated with palladium (Pd) using a sputter coater system to obtain a conductive

surface and reduce the incidence of charging, which is due to high negative charges accumulating on the sample surface. SEM was also used to examine the nanocomposite structure inside the dried polymeric coating surface.

FTIR spectroscopy was performed on the sample powders as well as on the obtained coating films using a Nicolet 6700 spectrophotometer (Thermo Electron Corporation) equipped with a diamond ATR Smart orbit window.

Spectra were obtained at  $1.0\text{ cm}^{-1}$  resolution averaging 32 scans to investigate and confirm the presence of ACP and VA within the polymeric coatings.

## 2.6. Adhesion test

The bond strength and stability of any coating on the substrate are a critical factor in determining its value to biomedical applications. Low-quality films could peel-off from the substrate when subjected to forces and loads, and thus, it is important to evaluate their adhesion properties. The adhesion of the polymeric coatings to the Ti substrate was evaluated according to the American Society for Testing Materials (ASTM) (Mittal, 1978)<sup>[62]</sup>. ASTM-D3359-02 tape test<sup>[63]</sup> was chosen to study the adhesion of polymeric coatings on the Ti alloy substrates. A crosscut pattern of 1 mm separation distance was made on the coating samples. An ASTM standard pressure sensitive tape was firmly adhered onto the coatings and then removed according to the procedure as described in the ASTM tape adhesion test.

## 2.7. Cell adhesion and cytocompatibility test

To test the cytocompatibility of the various ACP polymeric coatings, cell adhesion and live/dead tests were conducted. The influence of factors, such as ACP concentration and polymer type on osteoblast confluence and proliferation, was investigated. Murine osteoblast cell line, MC3T3-E1, was obtained from ATCC (Manassas, VA). Cells were cultured under  $37^{\circ}\text{C}$ , 5%  $\text{CO}_2$ , and 95% relative humidity in minimum essential medium ( $\alpha$ -MEM, Gibco, Grand Island, NY) containing 10 vol.% fetal bovine serum (FBS, Atlanta Biologicals, Lawrenceville, GA) and 1% penicillin-streptomycin solution (P/S, Gibco, Grand Island, NY). Cells at the third to seventh passage were used in this experiment. All the substrates were sterilized under UV radiation for at least 60 min. The sterilized substrates were placed in 12-well plates and MC3T3-E1 cells were seeded on them at a concentration of 120,000 cells/well. A 1 ml of media/cm<sup>2</sup> of surface area was used and the culture media were changed daily. The effect of ACP concentrations on the osteoblast viability was evaluated using the Alamar blue assay. This bioassay was designed to quantitatively measure

the viability of various human and animal cell lines<sup>[64]</sup>. Cell viability and adhesion on these coated substrates were also assessed using live/dead staining (Invitrogen, Live/Dead Staining Kit). The live and dead cells were visualized at days 1 and 3 post-seeding using a fluorescence microscope (Olympus-CKX41).

## 2.8. VA release measurements

### 2.8.1. Elution experiment

The coated substrates were placed in a sterile 24-well tissue culture plate with 2.0 ml of phosphate-buffered saline (PBS, Lonza, 1 $\times$ ) completely covering the coating ( $n = 3$  of each group) kept under  $37^{\circ}\text{C}$ , 5%  $\text{CO}_2$ , and 95% relative humidity. All the 2.0 ml solution from the wells were taken out and analyzed at each time point, and the wells were replenished with 2.0 ml of fresh PBS. The concentration of VA released at each time point was determined by measuring the absorbance at 280 nm, from which the concentration was calculated using a standard calibration curve<sup>[64-67]</sup>. The mass of VA released was then calculated using the values of measured concentration and actual collected sample volume.

### 2.8.2. Antibiotic activity study

The biological activity of the released VA was evaluated on *Staphylococcus aureus* (*S. aureus*) by measuring the zone of inhibition using the disk diffusion method. The objective of this test was to validate that the released VA is still active after the coating on the Ti substrates. *S. aureus* was purchased from the American Type Culture Collection (ATCC). *S. aureus* was pre-cultured with soy broth (BD Biosciences, NJ) at  $37^{\circ}\text{C}$  in a shaking incubator for 7 h and inoculated on a Mueller-Hinton agar plate. The blank antimicrobial susceptibility disks (Oxoid, UK) were placed on the bacteria plate and 10  $\mu\text{L}$  of the elutes collected from each group at various time intervals were then carefully loaded to these disks. The known concentrations of VA were used for the control. The plates were incubated overnight at  $37^{\circ}\text{C}$  and the area of microbial resistance was measured.

## 3. Results and discussion

### 3.1. Coating solution and parameters

The custom developed 3D printing technique was employed to coat all the substrates with different therapeutic agents in polymeric formulations. Monodispersed droplets as shown in Figure 2B were generated for polymeric solutions so that precision deposition was achieved on the Ti substrate.

The jetting performance of each candidate polymeric solution was dictated by the physical properties of the printing solutions, which were controlled by adjusting the

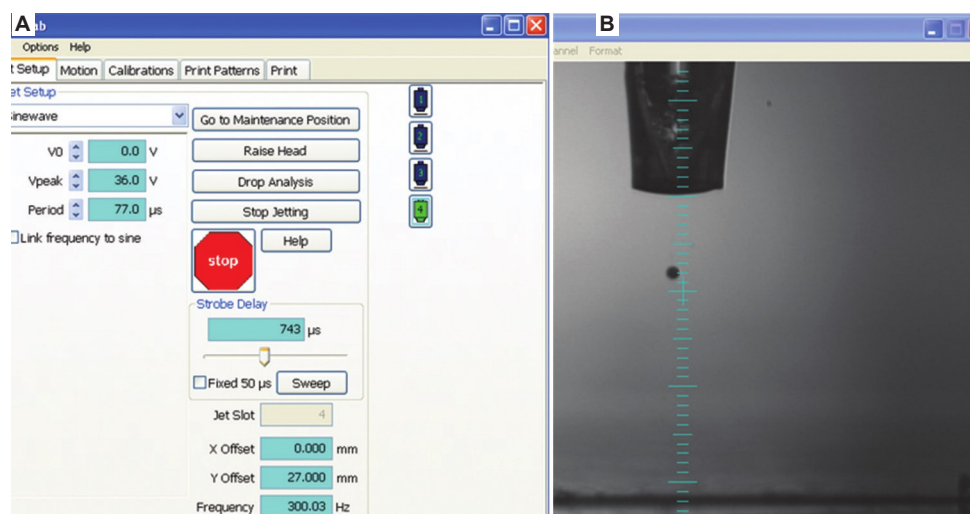


Figure 2. (A) Jetting parameters. (B) Single monodisperse droplet.

jetting parameters. Jetting parameters were optimized for droplet consistency, and the final jetting parameters were obtained at a reservoir pressure of  $-24$  psi, peak voltage ( $V_{peak}$ ) of 36 V, period of 77  $\mu$ s, and frequency of 300 Hz, as shown in Figure 2A. Figure 2B shows a monodisperse PCL/ACP solution drop being jetted from a 50  $\mu$ m nozzle orifice.

The rheological properties of the coating inks were measured to evaluate their printability using the customized inkjet printer. Figure 3 shows the variation in the Z number for different inks in this research. As can be seen, a reduction of Z number was observed as the ACP content increased for both PLGA and PCL polymers due to increase in the viscosity of the inks. Furthermore, PCL virgin ink had higher viscosity as compared to PLGA virgin ink due to higher molecular weight and long-range chains. However, it is noteworthy to point out that all the inks were within the jettability range of Z number  $-1-10$  without forming satellites.

### 3.2. Coating integrity and morphological characterization

The coating uniformity and surface morphology of the fabricated polymeric coatings were analyzed using optical microscopy and SEM, respectively. Under optical microscopy, PCL-ACP coatings displayed uniform deposition patterns and adherence with the Ti alloy substrate, as shown in Figure 4A and B. However, PLGA-ACP coatings had random deposition patterns, as depicted in Figure 4C and D. The PLGA-ACP coatings show spots on the Ti alloy substrate, which represent regions coated with bare PLGA polymer without the presence of ACP.

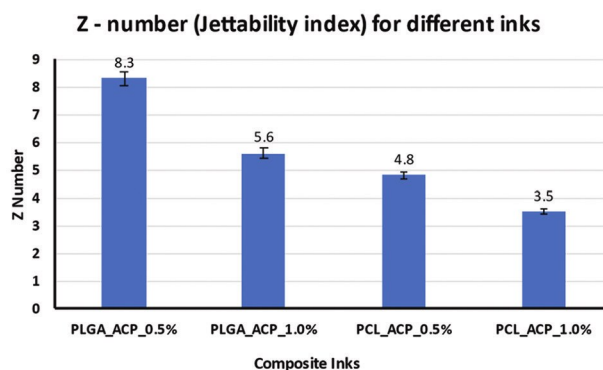


Figure 3. Printability of different composite polymer inks using Z number.

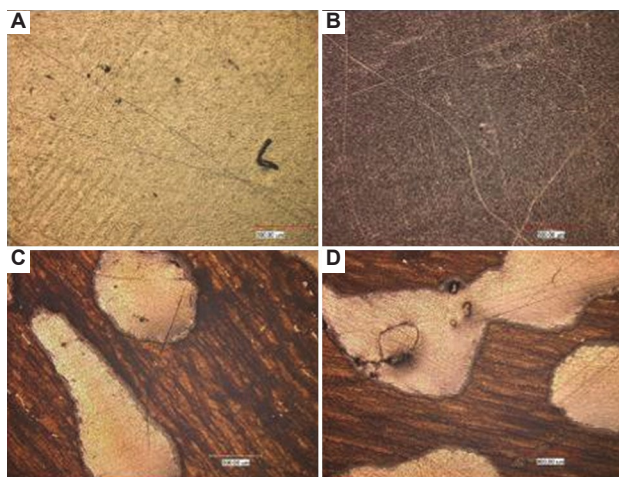


Figure 4. Optical microscopy of (A) Ti-1%PCL-0.5%ACP, (B) Ti-1%PCL-1%ACP, (C) Ti-1%PLGA-1%ACP, and (D) Ti-1%PLGA-0.5%ACP. Ti: Titanium, ACP: Amorphous calcium phosphate, PCL: Polycaprolactone, PLGA: Poly(lactic-co-glycolic) acid.

This can be attributed to the precipitation and saturation of the ACP within the coated regions.

On the contrary, the PCL-ACP-coated substrates have a uniform deposition (Figure 4A and 4B) pattern as seen under the optical microscope, which is desirable for orthopedic implant applications. Hence, SEM imaging was specifically conducted on the PCL-ACP-coated films and is shown in Figure 5. SEM images were taken at different magnifications. For all the PCL-ACP coatings, the micrographs indicated no defects, such as cracks or inclusions (Figure 5A-C). At a higher magnification (25k-X), the SEM image (Figure 5A) depicts the nanocomposite structure inside the coatings wherein the ACP particles are strongly bound to the PCL polymer. At lower magnifications, all the coatings exhibit uniform deposition pattern and adherence with the substrates, as shown in Figure 5D-F.

Figure 6 shows a multilayer (10 layers) 3D scaffold printed using composite polymer inks to demonstrate the fabrication of complex and hierarchical structures. These scaffolds were infiltrated with higher concentrations of ACP particulates as evident from the precipitated ACP structures on the surface. Thus, we have demonstrated selective *in situ* saturation of scaffold structures which can benefit different tissue types based on the cell seeding protocols. The customized 3D printing system employed in this research enables deposition of different geometries by exploiting material properties of inks to deposit a variety of 3D objects (tubular, planar, and stackable configurations). In addition, we have demonstrated the selective infiltration capability on these scaffolds. Thus, our combinatorial inkjet method enables 3D objects to have functionally gradient properties which are seldom achieved by stand-alone deposition processes. Traditional biomanufacturing

processes deliver high-quality structures, however, need further post-processing to achieve the desired functional properties which can be overcome by employing the customized inkjet process implemented in this research.

### 3.3. Chemical composition analysis

To investigate and characterize the conformation of the polymer, ACP or VA phases present in the coatings, FTIR was used. FTIR was performed on virgin polymers, ACP sample powders, as well as the polymeric-coated films for various experimental samples.

The X-ray diffraction (XRD) patterns of the powder used in this study are shown in Figure 7A. The absence of any crystalline peak confirms the formation and amorphous nature of ACP. The SEM image of the as prepared ACP powder is shown in Figure 7B. The SEM shows the formation of agglomerates consisting of extremely fine featureless spherical nanoparticles of calcium phosphate. The measured Brunauer-Emmett-Teller (BET)-specific surface area of this ACP powder was found to be  $60 \pm 2 \text{ m}^2/\text{g}$  which corresponds to a particle size of  $\sim 32 \text{ nm}$ . XRD along with SEM and BET results confirmed that the powder used in this study consists of nanoparticles of amorphous calcium phosphates.

Figure 8A and B shows the absorbance peaks that are superimposed for PCL and ACP within PCL-1%ACP and PCL-0.5%ACP-coated samples. The FTIR of the printed composite coating shows the presence of both the PCL and PLGA polymers and the ACP. Figure 8A and B confirms the presence of the PCL polymer ( $\text{C-H} \sim 2850 \text{ cm}^{-1}$ ,  $\text{C=O} \sim 1750 \text{ cm}^{-1}$ ) and ACP phase within the coatings. Similarly, Figure 8C and D shows the absorbance peaks that are superimposed for PLGA and ACP within PLGA-1%ACP

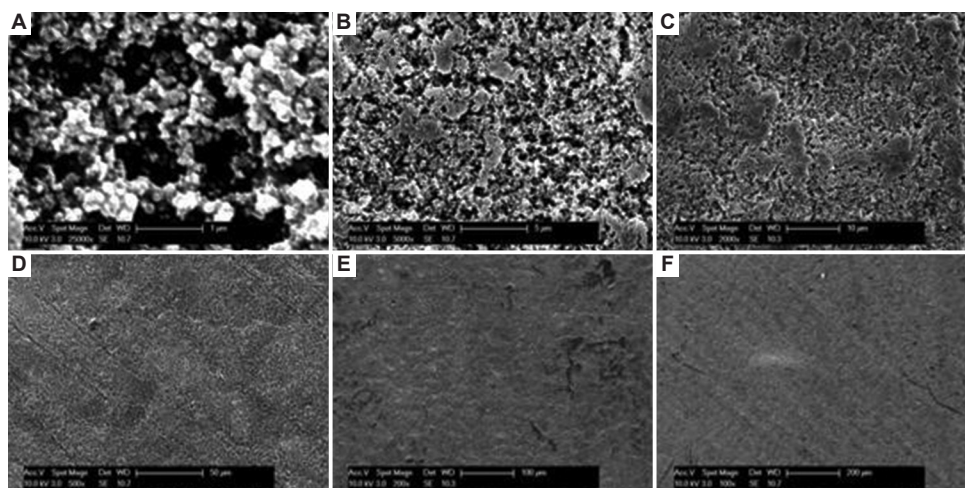


**Figure 5.** SEM micrographs of Ti-1%PCL-1%ACP at (A) 25k-X, (B) 5k-X, (C) 2k-X, (D) 0.5k-X, (E) 0.2k-X, and (F) 0.1k-X magnifications. SEM: Scanning electron microscopy, Ti: Titanium, PCL: Polycaprolactone, ACP: Amorphous calcium phosphate.

and PLGA-0.5%ACP-coated samples. The FTIR analysis confirms the presence of PLGA polymer (C-H  $\sim 2997\text{ cm}^{-1}$ , C=O  $\sim 1695\text{ cm}^{-1}$ ) and ACP phase within the coatings. In addition, the ACP peaks ( $\text{PO}_4^{3-}$  group  $\sim 1000\text{ cm}^{-1}$  and  $560\text{ cm}^{-1}$ ,  $\text{CO}_3^{2-}$  group  $\sim 1640\text{ cm}^{-1}$ )<sup>[68]</sup> are detected within the blended PCL-ACP and PLGA-ACP coatings.

### 3.4. Adhesion test

The bonding strength and stability of the coatings were evaluated according to the American Society for Testing Materials<sup>[62]</sup>. ASTM-D3359-02 tape test was chosen to study the adhesion of the various polymeric coatings on the substrates. A lattice pattern with 7 – 9 cuts in each direction was made in the polymeric film to the substrate. Pressure sensitive tape was then applied over the lattice and then peeled-off. Bond strength was evaluated by comparison with descriptions and illustrations as stated by the ASTM D3359-02 procedure<sup>[63]</sup>. Optical images

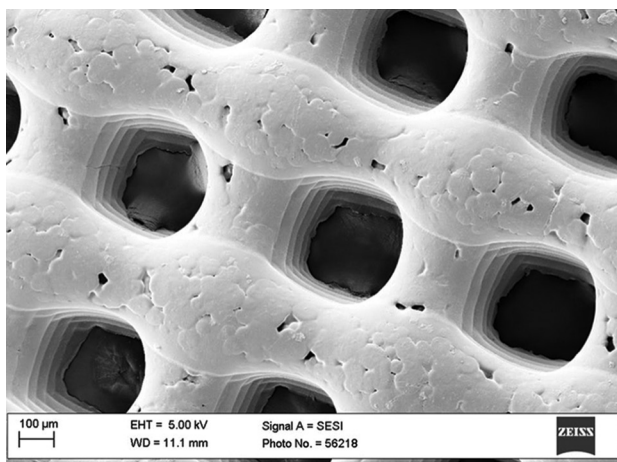


**Figure 6.** Scanning electron microscopy micrographs of multilayer 3D-printed scaffold using composite polymer media infiltrated with high concentration ACP inks. ACP: Amorphous calcium phosphate.

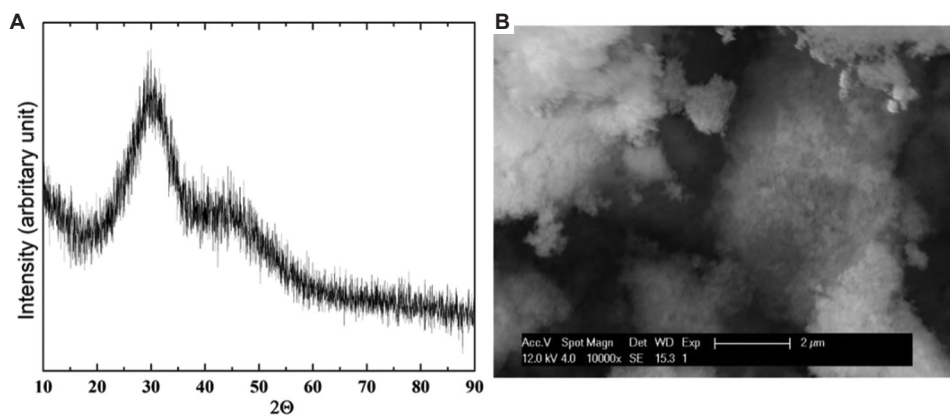


**Figure 7.** (A) X-ray diffraction patterns of the ACP powder. (B) Scanning electron microscopy image of ACP powder. ACP: Amorphous calcium phosphate.

obtained before and after applying the pressure sensitive tape to the polymeric-coated samples depicted coatings that were undetached from the substrates. This indicates a strong adhesion between polymeric coatings and Ti substrate. **Figure 9** shows an optical image before and after adhesion test for PCL-coated samples.

As seen in the optical images after bond test, all the coating was undetached after the removal of the pressure sensitive tape from the coated sample. A classification of “5B” (0% area removed) was assigned as the adhesion test results for each sample fabricated. This indicated that the polymeric coatings strongly adhered on the surface of the Ti alloy substrate.

### 3.5. Cytocompatibility tests

*In vitro* cell viability study results (**Figure 10**) indicate that all the coated samples are cytocompatible, and no significant differences were observed among the various coated samples. These results also indicate that the nature of the polymer and the amount of ACP present in the composite films do not affect the cell viability.

### 3.6. *In vitro* cytocompatibility assessment

To confirm the cellular viability data, cell viability was visualized by fluorescence imaging using live/dead staining. **Figure 11** shows the live/dead cells at 72 h (day 3) for the different polymeric coatings and positive controls (bare Ti). The PCL-ACP (sample codes: 1, 2, 5, and 6) coatings showed cellular attachment that was comparable to the positive controls. The number of layers for the PCL-ACP coating does not appear to have much influence on the cell attachment. This is also supported by the cell viability results (**Figure 10**), which show comparable viability for the 10 and 20 layers of PCL-ACP films. However, the PLGA-ACP coatings displayed regions with more dead cells and poor cell attachment, where the ACP phase was absent. We

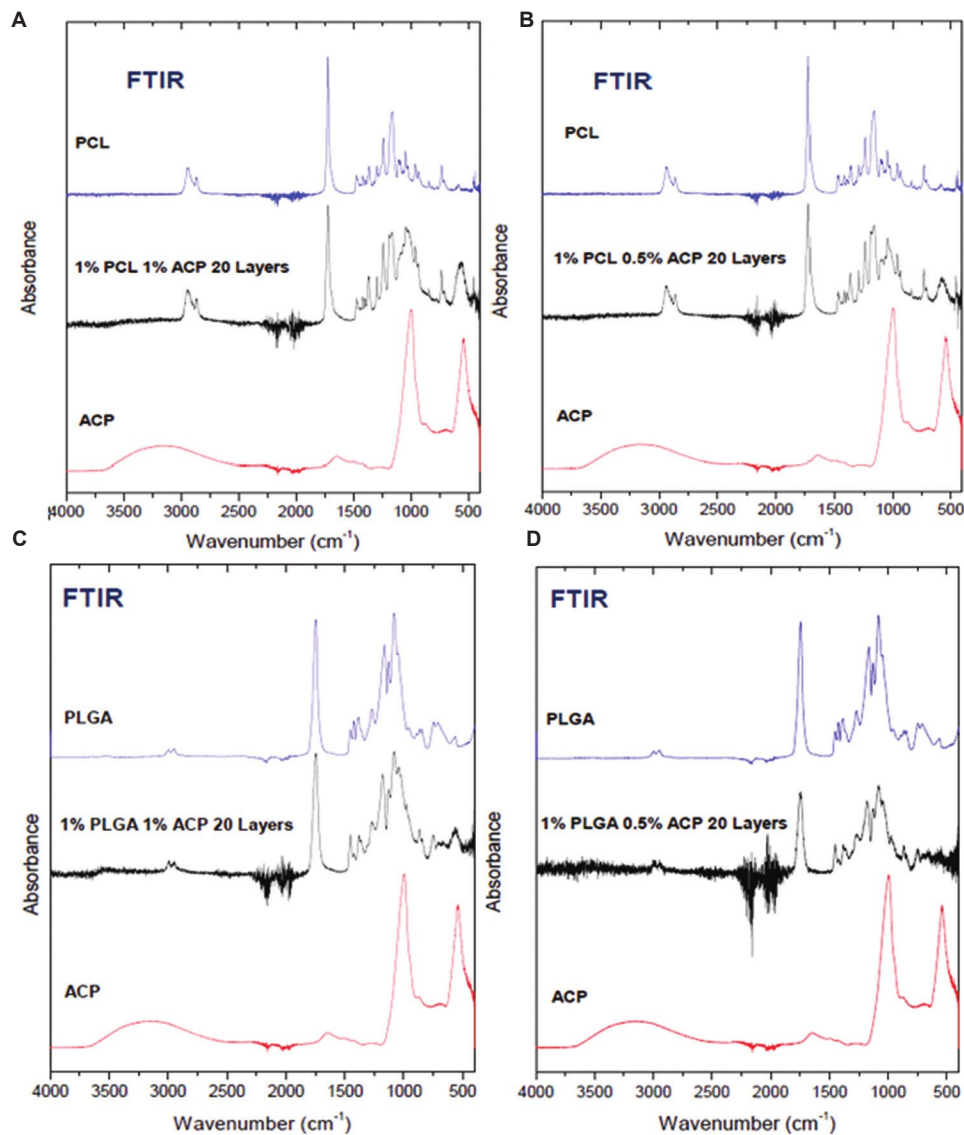


**Figure 8.** (A-D) FTIR of PCL-ACP and PLGA-ACP coatings. FTIR: Fourier transform infrared, PCL-ACP: Polycaprolactone-amorphous calcium phosphate, PLGA-ACP: Poly(lactic-co-glycolic) acid-amorphous calcium phosphate.

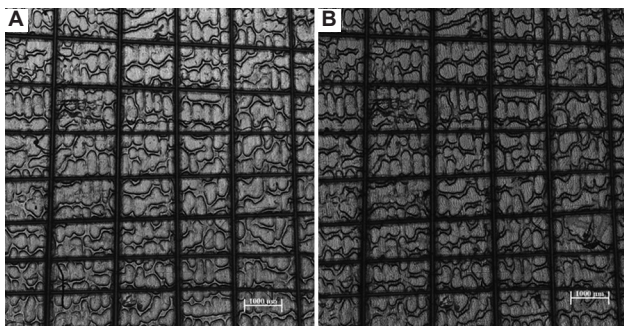


**Figure 9.** Optical images of PCL-ACP\_0.5% 10-layer coating on Ti substrate (A) before and (B) after adhesion test. PCL-ACP: Polycaprolactone-amorphous calcium phosphate.

correlated the PLGA-ACP cytocompatibility results with optical micrographs shown in [Figure 4C and D](#), which show PLGA-ACP coatings with regions of PLGA polymer without the ACP phase on the Ti substrate. This may be due to the local release of carboxylic acids produced through the degradation of PLGA, which increases the local acidity<sup>[69]</sup>. We have shown that the degradation of PLGA reduces the local pH drastically and, therefore, creates a zone which is cytotoxic. We have also shown that the presence of calcium phosphate can act as a buffering agent and help prevent a considerable decrease in pH<sup>[69]</sup>. A more physiological pH favors the cell attachment and hence, more live cells can be found in the composite films

of PLGA-ACP. Except for the very few of these localized depositions of the PLGA patches, the rest of the film allows the cells to attach and proliferate. The high % viability of these PLGA-ACP films (Figure 10) clearly demonstrates that these PLGA-rich zones have hardly any effect on the overall cell viability and proliferation.

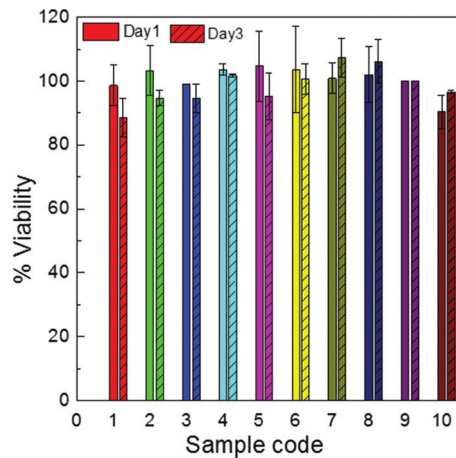


**Figure 10.** *In vitro* viability assessment using MC3T3 cells after 24 h (day 1) and 72 h (day 3) of culture. Sample codes for samples 1 – 8 are given in Table 1. Samples 9 and 10 are Ti substrate and tissue culture dish, respectively. The % viability values of the samples were normalized with respect to the Ti substrate. Ti: Titanium.

The presence of ACP in the printed films, however, offers some unique advantages other than buffering the local pH. It is well-known that ACP has the highest solubility among the various calcium phosphate phases, and therefore, it is expected to dissolve and release calcium and phosphate ions in the system<sup>[70]</sup>. Moreover, the protons generated from the released acidic byproducts of PCL and PLGA interact with the ACP particles, leading to an increase in dissolution of the ACP particles which also causes an increase in the concentrations of soluble  $\text{Ca}^{2+}$  and phosphate in the surrounding media. It is well-established that the release of calcium and phosphate ions locally improves the osteoclast and osteoblast activity, which, in turn, facilitates bone regeneration<sup>[71,72]</sup>. Thus, it is expected that the composite films of PCL-ACP and PLGA-ACP should demonstrate improved biological response as compared to the polymers film alone.

### 3.7. Antibiotic drug release kinetics

The *in vitro* release kinetics of the VA from the coated samples R-1, R-2, and R-3 samples (Table 2) was measured in PBS and is shown in Figure 12A. The samples R-1 and R-2 showed burst release at the beginning and the release profiles were very similar. Both samples showed a cumulative release of 80% within the first 8 h of elution. After this initial burst, the release was slow and almost

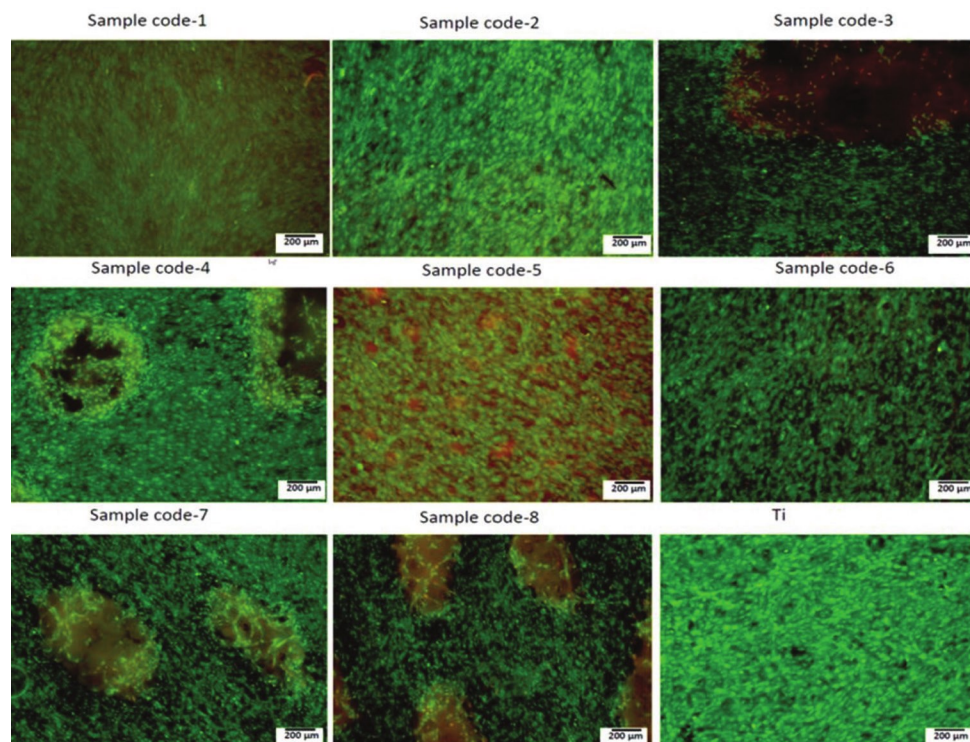


**Figure 11.** *In vitro* cytocompatibility assessment (live/dead tests) using MC3T3 cells at day 3 for different samples. Sample codes for samples 1 – 8 are given in Table 1.

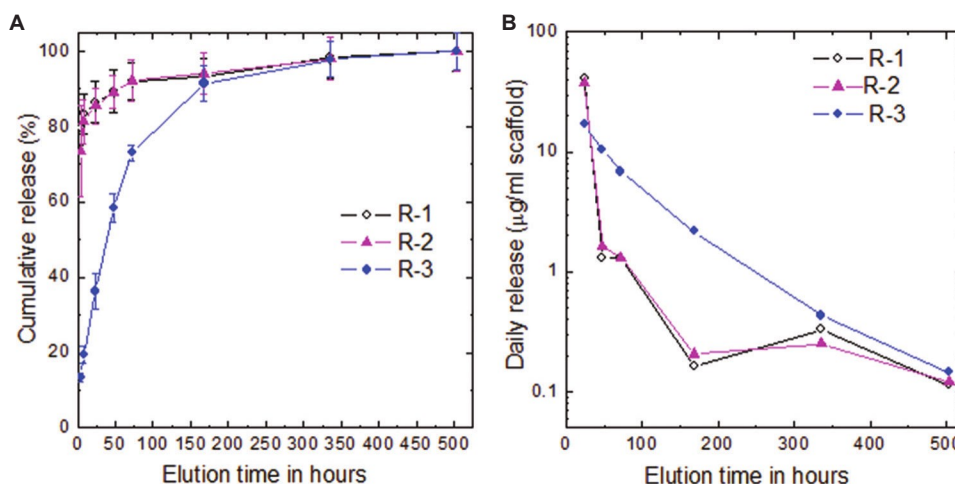


Figure 12. Vancomycin release kinetics from coated samples. (A) Cumulative release %. (B) Daily release.

all the VA (>98%) was released within 336 h (14 days) of elution. The sample R-3 showed much slower release than R-1 and R-2, and only 20% of VA was released within 8 h with 60% being released after 72 h. However, like the other samples, almost all the incorporated VA was released within 336 h of elution. The daily release of VA for all the samples is shown in Figure 12B. It is clear that the amount of VA released per day is below 2 mg/ml after 1 day and below 1 mg/ml after 48 h of elution for samples R-1 and R-2. Similar to Figure 12A, sample R-3 showed sustained release of VA and the amount of VA released per day was above 2 mg/ml for the first 7 days (168 h).

It is known that VA is an important antibiotic for the effective treatment of severe bone infections caused by Gram-positive bacteria, such as *S. aureus*<sup>[66,73,74]</sup>. Moreover, compared to other antibiotics, VA does not interfere much with osteoblast and skeletal cell growth *in vitro*<sup>[75,76]</sup> and, additionally, does not affect the bone regeneration process *in vivo*<sup>[77,78]</sup>. For an effective treatment, the delivery mechanism should be able to release VA for a prolonged time well above the MIC and preferable above the minimum bactericidal concentration (MBC). The MIC and MBC values of VA are in the range of 0.75–2 µg/ml and ~ 8 µg/ml, respectively<sup>[66,79,80]</sup>. Samples R-1 and R-2 showed VA release concentrations above MIC value only in the first 48 h of release and the concentration goes down below 1 µg/ml beyond this time (Figure 12B). Sample R-3 showed a sustained release of VA above MIC for 7 days.

Table 3 shows the different stages of drug elution and respective cumulative release for each sample type. Samples R-1 and R-2 exhibit identical drug elution behavior with substantial (89%) release occurring in the initial 50 h, whereas sample R-3 shows a relatively lower burst release

Table 3. Vancomycin release kinetics at different phases of drug elution.

Drug release phase	Time (h)	Cumulative release (%)	
		R1 and R2	R3
Initial burst	50	89	40
Terminal burst	80	93	62
Transition state	160	95	92
Steady state	400	98	98

phenomena with only 40% drug elution during the initial burst phase. At terminal burst stage (80 h), R-1 and R-2 show a marginal increase in drug elution (4%) as compared to a higher elution (22%) in sample R-3. During the transition state (160 h), all samples approach a tapering release phase. Finally, at the steady state phase, all the samples have eluted 98% of the drug content. The cumulative release profile (Figure 12A), daily release profile (Figure 12B), and the total amount of VA entrapped in the coatings of samples R-1 and R-2 are very similar and this is not surprising as the number of layers was halved, and concentration of VA was doubled in R-2 sample compared to R-1. These results also demonstrate the reproducibility of the direct writing process. Based on this, one should expect that the VA entrapped in the sample R-3 should be almost twice that of R-1 and R-2. However, the total amount of VA entrapped in the R-3 sample was very similar to R-1 and R-2. This may be due to the inhomogeneous coating process that occurred with ACP containing solution (Figure 4C and D) as has been discussed previously.

The release profiles of samples R-1 and R-2 are also very different from that of sample R3, and the latter showed much more sustained release over time comparatively.

The fast degradation of PCL in contact with the buffer or presence of free VA particles on the film surface due to the poor encapsulation of VA inside the PCL films most likely caused the burst release of VA at the beginning of elution for samples R-1 and R-2. However, the degradation of PCL under physiological buffers has shown to be very slow, and therefore, rapid dissolution of the inadequately encapsulated VA causes the burst release<sup>[81]</sup>. Moreover, this rapid dissolution of the VA should create pores within the PCL matrix. In the latter time points, the rest of the VA molecules and water molecules diffuse through these pores and should give a more sustained release<sup>[82]</sup>. Since ~80% of the VA was released within 8 h of elution, it can, therefore, be concluded that most VA particles were poorly encapsulated by PCL<sup>[83]</sup>. This is not very surprising as the PCL concentration that was used for the coating in this study was only 1% by weight, which may be too low to encapsulate the VA particles effectively. PCL has been used to coat  $\beta$ -tricalcium phosphate composites, and it has been shown that higher PCL-containing coatings delay the release of VA<sup>[84]</sup>. The above argument of poor VA encapsulation, however, does not hold for the sample R-3, which showed much-sustained release of VA over time. This can be explained by assuming the adsorption of VA on the surfaces of the nanocrystalline ACP particles. The ACP powder used in this study has a BET surface area of ~61 m<sup>2</sup>/g, which corresponds to spherical particles of ~32 nm in size. It is well-established in the literature that these nanosized calcium phosphate particles also exhibit surface roughness and topographic irregularities on the atomic scale, which favor adsorption, promoting facile formation and retention of stable aggregates even under relatively intensive agitations in the solution<sup>[85-87]</sup>.

The initial burst release around the implant area is extremely important and concentration of the released VA should reach well above the MBC of ~8  $\mu$ g/ml. This high concentration of VA ensures the complete eradication of Gram-positive bacteria from the surrounding tissues and the surface of the implant. The controlled slow release of VA above MIC after this initial burst is also critical to further eliminate any reinfection or growth of bacteria around the implant. Suboptimal release of VA below MBC at the initial stage may cause the bacteria to survive for a long time although they may not grow due to the release of VA concentration above the MIC. This sub-dose release of VA may lead to the reinfection or chronic infection of the wound, which drastically enhances the possibility of implant failure and wound infection-related complications.

It is also reported that due to the alternation of charged Ca<sup>2+</sup> and PO<sub>4</sub><sup>3-</sup> ions of calcium phosphate surfaces, the surfaces adsorb both acidic and alkaline protein, DNA, and biomolecules, regardless of their actual  $\zeta$ -potential

and net charge<sup>[85,88]</sup>. Thus, the adsorption of VA molecules on the surfaces of nanosized ACP particles is highly feasible. On contact with water, some of these adsorbed VA molecules diffused out in the solution, thereby resulting in a more sustained release in sample R-3. The decrease in the rate of release of VA over time is presumed partially due to the reduction in easily soluble amorphous content of the ACP powder on the particle surface, combined with the conversion of the ACP phase into hydroxyapatite by dissolution precipitation as well as the strongly adsorbed drug molecules on the particle surface<sup>[85,89]</sup>.

The bioactivity of the VA released from different coated samples between specific time points was measured by measuring the zone of inhibition using the disc diffusion method and is shown in Figure 13. Known concentrations of freshly prepared VA solutions were used as the control (Figure 13A-H). Figure 13 clearly shows that the VA released from the coated samples is bioactive. Moreover, similar concentration of VA, either from the control or from the coated samples, yielded similar values of zone of inhibition diameters (Figure 13B and E), confirming that the direct writing process does not affect the bioactivity of the VA during the printing process. The zone of inhibition diameter decreases considerably with the decrease in the VA concentration, and no noticeable zone of inhibition was observed for VA concentrations below 10  $\mu$ g/ml (Figure 13A-H).

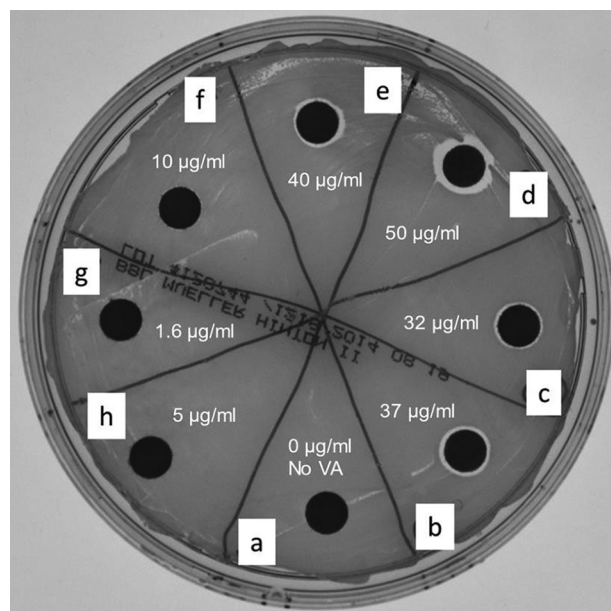


**Figure 13.** Zone of inhibition induced by elutes from the controls and the various coated samples (A) Control-1: no VA, (B) VA released from R-1 between 0 and 4 h. (~37  $\mu$ g/ml), (C) VA released from R-2 between 0 and 4 h. (~32  $\mu$ g/ml), (D) Control-2: 50  $\mu$ g/ml of VA, (E) Control-3: 40  $\mu$ g/ml, (F) VA released from R-3 between 24 and 48 h. (~10  $\mu$ g/ml), (G) VA released from R-2 between 24 and 48 h. (~1.6  $\mu$ g/ml), (H) Control-3: 5  $\mu$ g/ml. VA: Vancomycin.

## 4. Discussion

In our past work, direct-write polymeric coatings have been implemented to retard the corrosion behavior of magnesium alloy for tracheal stent application. Similarly, inkjet printing has provided controlled release coatings for drug-eluting cardiovascular stents. In contrast, in the current research, a customized and retrofitted direct-write inkjet method was employed to deposit bioactive organic-inorganic composite thin films on Ti alloy substrates. We deposited multilayered coatings (10 layers) 3D scaffold printed using composite polymer inks to demonstrate the fabrication of complex and hierarchical structures. Optimal jetting conditions suitable for both PCL and PLGA polymer types were used for coating multilayer polymeric thin films. The biopolymers were blended with nanostructured amorphous calcium phosphate and VA drug for promoting osteoconductivity and preventing bacterial infection associated with orthopedic implants. The customized 3D printing process enabled the deposition of multilayered coatings with precise control on the thickness of these films to obtain tunable release of the ACP *in vitro*. Optical microscopy revealed that PCL-ACP coatings had uniform deposition patterns, whereas the PLGA-ACP coatings displayed precipitation of ACP patches on the Ti substrate. Further SEM analysis of the nanocomposite structure within the polymeric coatings revealed a strong binding between the ACP nanoparticulate and PCL polymer. The FTIR analysis confirmed the presence of both the polymers and ACP phases within the multilayered thin films<sup>[24]</sup>. The MC3T3 osteoblast cell line showed high cellular viability (>90%) after 72 h of proliferation, which was comparable to Ti substrate and TCPS controls. The cell attachment and live/dead assay confirmed the cell viability data. However, PLGA coatings had poor cellular attachment (dead cells) in certain regions of the substrate. These findings indicate the local release of carboxylic acids produced through degradation of PLGA increases the local acidity<sup>[50]</sup>. The presence of ACP in the printed films, however, offers some unique advantages other than buffering the local pH. It is known that ACP has the highest solubility among the various calcium phosphate phases, and it is expected to dissolve and release calcium and phosphate ions in the system. Moreover, the protons generated from the released acidic byproducts of PCL and PLGA interact with the ACP particles, leading to an increase in dissolution of the ACP particles which also causes an increase in the soluble  $\text{Ca}^{2+}$  and phosphate concentrations in the surrounding media. It is well-established that the release of calcium and phosphate ions locally improves the osteoclast and osteoblast activity, thereby facilitating bone regeneration<sup>[16]</sup>. Thus, it is expected that the composite films of PCL-ACP and PLGA-ACP should demonstrate

improved biological response as compared to the polymers film alone.

The VA release data revealed that PCL-ACP composite films showed slow release compared to PCL film alone. This is due to the adsorption of VA molecules on the surfaces of nanosized ACP particles. Moreover, compared to other antibiotics, VA did not interfere much with osteoblast and skeletal cell growth *in vitro* and did not affect the bone regeneration process *in vivo*<sup>[13]</sup>. The ACP powder used in this study had a BET surface area of  $\sim 61 \text{ m}^2/\text{g}$ , which corresponds to spherical particles of  $\sim 32 \text{ nm}$  in size. It is well-established in the literature that these nanosized calcium phosphate particles also exhibit surface roughness and topographic irregularities on the atomic scale, which favor adsorption, promoting facile formation, and retention of stable aggregates even under relatively intensive agitations in the solution<sup>[52]</sup>. It is also reported that due to the alternation of charged  $\text{Ca}^{2+}$  and  $\text{PO}_4^{3-}$  ions on calcium phosphate surfaces, the surfaces adsorb both acidic and alkaline proteins, DNA, and biomolecules, regardless of their actual  $\zeta$ -potential and the net charge<sup>[26,52]</sup>. Thus, the adsorption of VA molecules on the surfaces of nanosized ACP particles is highly feasible. On contact with water, some of these adsorbed VA molecules diffused out in the solution and thus resulted in a more sustained release in sample R-3. Presumably, the decrease in the rate of release of VA over time is partly due to the reduction in easily soluble amorphous content of the powder on the particle surface, combined with the conversion of the ACP phase into hydroxyapatite by dissolution precipitation and corresponding decrease in the concentration of weakly adsorbed drug molecules on the particle surface<sup>[2,52]</sup>.

The bioactivity of the released VA was confirmed by measuring the zone of inhibition using the disc diffusion method. Thus, the direct-write printing method successfully immobilized therapeutic agents on orthopedic implants for the temporospatial release of drugs. This research, therefore, builds the foundation for incorporating bioactive agents within the polymeric coating to efficiently regenerate bone structures that interface with orthopedic implants and prevent bacterial infection resulting from implantation.

## 5. Conclusions

In this study, a custom 3D printing method was employed to deposit bioactive organic-inorganic composite thin films on Ti alloy substrates. Optimal jetting conditions suitable for both PCL and PLGA polymer types were used for coating multilayer polymeric thin films. The biopolymers were blended with nanostructured amorphous calcium phosphate and VA for promoting osteoconductivity and

preventing bacterial infection associated with orthopedic implants. The direct-write process enabled the precise control on the thickness of these films to obtain tunable release of the ACP *in vitro*. Optical microscopy revealed that PCL-ACP coatings had uniform deposition patterns, whereas the PLGA-ACP coatings displayed precipitation of ACP patches on the Ti substrate. Further SEM analysis of the nanocomposite structure within the polymeric coatings revealed a strong binding between the ACP nanoparticulate and PCL polymer. The FTIR analysis confirmed the presence of both polymers and ACP phases within the multilayered thin films. The MC3T3 osteoblast cell line showed high cellular viability (>90%) after 72 h of proliferation, which was comparable to Ti substrate and TCPS controls. The cell attachment and live/dead assay confirm the cell viability data. However, PLGA coatings had poor cellular attachment (dead cells) in certain regions of the substrate. These findings correlate well with optical micrographs for PLGA-ACP coatings, which show regions of PLGA polymer without ACP phase due to irregular precipitation. The VA release data revealed that the PCL-ACP composite films showed slow release compared to PCL film alone. This is due to the adsorption of VA molecules on the surfaces of nanosized ACP particles. Moreover, the bioactivity of the released VA was confirmed by measuring the zone of inhibition using disk diffusion method. All these results confirmed that the direct-write printing method can be successfully used to immobilize drugs on orthopedic implants and can be employed for temporospatial control release of these drugs. This research, therefore, lays a foundation for incorporating bioactive agents within the polymeric coating to efficiently regenerate bone structures that interface with orthopedic implants and prevent bacterial infection resulting from implantation.

## Acknowledgments

The authors would like to thank the NSF Engineering Research Center for Revolutionizing Metallic Biomaterials (NSF-EEC award 0812348) and NSF-CMMI awards (2100739, 1663128, 2100850) for support toward this research. We would also like to thank the Center of Excellence in Product Design and Advanced Manufacturing at North Carolina A&T State University for its support toward this research. PNK also acknowledges the financial support of the Edward R. Weidlein Endowed Chair Professorship funds and the Center for Complex Engineered Multifunctional Materials (CCEMM), Swanson School of Engineering, and the University of Pittsburgh for partial support of this research.

## Funding

The authors would like to express their gratitude for funding support from the National Science Foundation Grant (NSF

CMMI Award #1663128, #2100739, #2100850) and the Center of Excellence in Product Design and Advanced Manufacturing at North Carolina A&T State University.

## Conflict of interest

The authors declare that they have no conflicts of interest. The funders had no role in the design of the study; in the collection, analyses, or interpretation of data; in the writing of the manuscript, or in the decision to publish the results.

## Author contributions

*Conceptualization:* Eben Adarkwa, Abhijit Roy, Prashant N. Kumta, and Salil Desai

*Formal analysis:* Eben Adarkwa, Abhijit Roy, and Salil Desai

*Funding acquisition:* Prashant N. Kumta and Salil Desai

*Investigation:* Eben Adarkwa, Abhijit Roy, John Ohodnicki, Boeun Lee, and Salil Desai

*Methodology:* Eben Adarkwa, Abhijit Roy, Prashant N. Kumta, and Salil Desai

*Supervision:* Prashant N. Kumta and Salil Desai

*Writing – original draft:* Eben Adarkwa, Abhijit Roy, and Salil Desai

*Writing – review & editing:* Eben Adarkwa, Abhijit Roy, Prashant N. Kumta and Salil Desai

All authors have read and agreed to the published version of the manuscript.

## Ethics approval and consent to participate

Not applicable.

## Consent for publication

Not applicable.

## Availability of data

The data presented in this study are available on request from the corresponding author.

## References

1. Bose S, Robertson SF, Bandyopadhyay A, 2018, Surface modification of biomaterials and biomedical devices using additive manufacturing. *Acta Biomater*, 66: 6–22.  
<https://doi.org/10.1016/j.actbio.2017.11.003>
2. Xue P, Li Q, Li Y, *et al.*, 2017, Surface modification of poly(dimethylsiloxane) with polydopamine and hyaluronic acid to enhance hemocompatibility for potential applications in medical implants or devices. *ACS Appl Mater Interfaces*, 9: 33632–33644.  
<https://doi.org/10.1021/ACSAMI.7B10260>

3. Xiao M, Chen YM, Biao MN, *et al.*, 2017, Bio-functionalization of biomedical metals. *Mater Sci Eng C Mater Biol Appl*, 70: 1057–1070.  
<https://doi.org/10.1016/J.MSEC.2016.06.067>
4. Adarkwa E, Kotoka R, Desai S, 2021, 3D printing of polymeric coatings on AZ31 Mg alloy substrate for corrosion protection of biomedical implants. *Med Dev Sens*, 4: e10167.  
<https://doi.org/10.1002/MDS3.10167>
5. Desai S, Shankar MR, 2021, Emerging trends in polymers, composites, and nano biomaterial applications. In: *Bio-Materials and Prototyping Applications in Medicine*. Germany: Springer. p.19–34.  
[https://doi.org/10.1007/978-3-030-35876-1\\_2](https://doi.org/10.1007/978-3-030-35876-1_2)
6. Aldawood FK, Andar A, Desai S, 2021, A comprehensive review of microneedles: Types, materials, processes, characterizations and applications. *Polymers (Basel)*, 13: 2815.  
<https://doi.org/10.3390/POLYM13162815>
7. Parupelli SK, Aljohani A, Khanal K, *et al.*, 2019, Direct Jet Printing and Characterization of Calcium Alginate Microcapsules for Biomedical Applications. In: *IIE Annual Conference Proceedings*. United States: Institute of Industrial and Systems Engineers (IISE). pp.300–305.
8. Marquetti I, Desai S, 2018, Molecular modeling the adsorption behavior of bone morphogenetic protein-2 on hydrophobic and hydrophilic substrates. *Chem Phys Lett*, 706: 285–294.  
<https://doi.org/10.1016/J.CPLETT.2018.06.015>
9. Marquetti I, Desai S, 2018, Adsorption behavior of bone morphogenetic Protein-2 on a graphite substrate for biomedical applications. *Am J Eng Appl Sci*, 11: 1037–1044.  
<https://doi.org/10.3844/AJEASSP.2018.1037.1044>
10. Aljohani A, Desai S, 2018, 3D printing of porous scaffolds for medical applications. *Am J Eng Appl Sci*, 11: 1076–1085.  
<https://doi.org/10.3844/AJEASSP.2018.1076.1085>
11. Biomedical Applications of Titanium and its Alloys. Available from: <https://www.tms.org/jom.html> [Last accessed on 2022 Mar 27].
12. Niinomi M, 2002, Recent metallic materials for biomedical applications. *Metallurgical Mater Trans A* 33: 477–486.  
<https://doi.org/10.1007/S11661-002-0109-2>
13. Desai S, Bidanda B, Bártolo P, 2008, Metallic and ceramic biomaterials: Current and future developments. In: *Bio-Materials and Prototyping Applications in Medicine*. Berlin: Springer. pp.1–14.  
[https://doi.org/10.1007/978-0-387-47683-4\\_1](https://doi.org/10.1007/978-0-387-47683-4_1)
14. Gu Y, Chen X, Lee JH, *et al.*, 2012, Inkjet printed antibiotic- and calcium-eluting bioresorbable nanocomposite micropatterns for orthopedic implants. *Acta Biomater*, 8: 424–431.  
<https://doi.org/10.1016/J.ACTBIO.2011.08.006>
15. Benoit MA, Mousset B, Delloye C, *et al.*, 1998, Antibiotic-loaded plaster of Paris implants coated with poly lactide-co-glycolide as a controlled release delivery system for the treatment of bone infections. *Int Orthop*, 21: 403.  
<https://doi.org/10.1007/S002640050195>
16. Dion A, Langman M, Hall G, *et al.*, 2005, Vancomycin release behaviour from amorphous calcium polyphosphate matrices intended for osteomyelitis treatment. *Biomaterials*, 26: 7276–7285.  
<https://doi.org/10.1016/J.BIOMATERIALS.2005.05.072>
17. Tang LH, Zhao CH, Xiong Y, *et al.*, 2009, Preparation, release profiles, and antibacterial properties of vancomycin-loaded poly(D,L-lactic) titanium alloy plates. *Orthopedics*, 32: 324.  
<https://doi.org/10.3928/01477447-20090501-16>
18. Jiang J, Li YF, Fang TL, *et al.*, 2012, Vancomycin-loaded nano-hydroxyapatite pellets to treat MRSA-induced chronic osteomyelitis with bone defect in rabbits. *Inflamm Res*, 61: 207–215.  
<https://doi.org/10.1007/S00011-011-0402-X/FIGURES/6>
19. Soundrapandian C, Datta S, Sa B, 2007, Drug-eluting implants for osteomyelitis. *Crit Rev Ther Drug Carrier Syst*, 24: 493–545.  
<https://doi.org/10.1615/critrevtherdrugcarriersyst.V24.16.10>
20. Zhao L, Chu PK, Zhang Y, *et al.*, 2009, Antibacterial coatings on titanium implants. *J Biomed Mater Res B Appl Biomater*, 91: 470–480.  
<https://doi.org/10.1002/JBM.B.31463>
21. Hetrick EM, Schoenfisch MH, 2006, Reducing implant-related infections: Active release strategies. *Chem Soc Rev*, 35: 780–789.  
<https://doi.org/10.1039/B515219B>
22. Lewis K, 2007, Persister cells, dormancy and infectious disease. *Nat Rev Microbiol*, 5: 48–56.  
<https://doi.org/10.1038/NRMICRO1557>
23. Dunne WM, 2002, Bacterial adhesion: Seen any good biofilms lately? *Clin Microbiol Rev*, 15: 155–166.  
<https://doi.org/10.1128/CMR.15.2.155-166.2002>
24. Antimicrobial and Wound Healing Properties of Nitric Oxide-Releasing Xerogels and Silica Nanoparticles Carolina Digital Repository, Dissertation or Thesis. p.47429941z. Available from: <https://www.cdr.lib.unc.edu/concern/dissertations/47429941z> [Last accessed on 2022 Mar 27].
25. Schairer DO, Chouake JS, Nosanchuk JD, *et al.*, 2012, The potential of nitric oxide releasing therapies as antimicrobial

- agents. *Virulence*, 3: 271.  
<https://doi.org/10.4161/VIRU.20328>
26. Desai S, Perkins J, Harrison BS, *et al.*, 2010, Understanding release kinetics of biopolymer drug delivery microcapsules for biomedical applications. *Mater Sci Eng B*, 168: 127–131.  
<https://doi.org/10.1016/J.MSEB.2009.11.006>
27. Marquetti I, Desai S, 2022, An atomistic investigation of adsorption of bone morphogenetic Protein-2 on gold with nanoscale topographies. *Surfaces*, 5: 176–185.  
<https://doi.org/10.3390/SURFACES5010010>
28. Marquetti I, Desai S, 2022, Nanoscale topographical effects on the adsorption behavior of bone morphogenetic Protein-2 on graphite. *Int JMol Sci*, 23: 2432.  
<https://doi.org/10.3390/IJMS23052432>
29. Marquetti I, Desai S, 2019, Orientation effects on the nanoscale adsorption behavior of bone morphogenetic Protein-2 on hydrophilic silicon dioxide. *RSC Adv*, 9: 906–916.  
<https://doi.org/10.1039/C8RA09165J>
30. Desai S, Bidanda B, Bártolo PJ, 2021, Emerging trends in the applications of metallic and ceramic biomaterials. In: *Bio-Materials and Prototyping Applications in Medicine*. Berlin: Springer. pp.1-17.  
[https://doi.org/10.1007/978-3-030-35876-1\\_1](https://doi.org/10.1007/978-3-030-35876-1_1)
31. Laser Fabrication of Polymeric Microneedles for Transdermal Drug Delivery DOE PAGES. Available from: <https://www.par.nsf.gov/biblio/10297495> [Last accessed on 2022 Apr 08].
32. Rodrigues J, Desai S, 2019, The nanoscale leidenfrost effect. *Nanoscale*, 11: 12139–12151.  
<https://doi.org/10.1039/C9NR01386E>
33. Gaikwad A, Desai S, 2021, Molecular dynamics investigation of the deformation mechanism of gold with variations in mold profiles during nanoimprinting. *Materials (Basel)*, 14: 2548.  
<https://doi.org/10.3390/MA14102548>
34. Desai SS, Marquetti I, Desai S, 2016, Molecular Modeling of Biochemical Cues Using High Performance Computing Molecular Modeling of biochemical cues using High Performance GPU. Available from: <https://www.researchgate.net/publication/316656312> [Last accessed 2022 Apr 07].
35. Cordeiro J, Desai S, 2017, The effect of water droplet size, temperature, and impingement velocity on gold wettability at the nanoscale. *JMicro Nano Manuf*. 25: 031008.  
<https://doi.org/10.1115/1.4036891/369684>
36. Neut D, Kluin OS, Crielaard BJ, *et al.*, 2009, A biodegradable antibiotic delivery system based on poly-(trimethylene carbonate) for the treatment of osteomyelitis. *Acta Orthop*, 80: 514.  
<https://doi.org/10.3109/17453670903350040>
37. Price JS, Tencer AF, Arm DM, *et al.*, Controlled release of antibiotics from coated orthopedic implants. *J Biomed Mater Res*, 30: 281–286.  
[https://doi.org/10.1002/\(SICI\)1097-4636\(199603\)30:3](https://doi.org/10.1002/(SICI)1097-4636(199603)30:3)
38. Lucke M, Wildemann B, Sadoni S, *et al.*, 2005, Systemic versus local application of gentamicin in prophylaxis of implant-related osteomyelitis in a rat model. *Bone*, 36: 770–778.  
<https://doi.org/10.1016/J.BONE.2005.01.008>
39. Sánchez E, Baro M, Soriano I, *et al.*, 2001, *In vivo-in vitro* study of biodegradable and osteointegrable gentamicin bone implants. *Eur JPharm Biopharm*, 52: 151–158.  
[https://doi.org/10.1016/S0939-6411\(01\)00169-2](https://doi.org/10.1016/S0939-6411(01)00169-2)
40. Perkins J, Xu Z, Roy A, *et al.*, 2014, Polymeric Coatings for Biodegradable Implants. Montreal, CANADA: AES-ATEMA 17th International Conference Advances and Trends in Engineering Materials and their Applications.
41. Perkins J, Desai S, Xu Z, *et al.*, 2012, Controlling Corrosion Mechanism of Biodegradable Magnesium Alloys for Implant Applications. In: *IIE Annual Conference Proceedings*. United States: Institute of Industrial and Systems Engineers (IISE). p.1.
42. Perkins J, Desai S, Wagner W, *et al.*, 2011, Biomanufacturing: Direct-writing of Controlled Release Coatings for Cardiovascular (Stents) Applications. In *IIE Annual Conference Proceedings*. United States: Institute of Industrial and Systems Engineers (IISE). p. 1.
43. Jiang T, Munguia-Lopez JG, Flores-Torres S, *et al.*, 2019, Extrusion bioprinting of soft materials: An emerging technique for biological model fabrication. *Appl Phys Rev*, 6: 011310.  
<https://doi.org/10.1063/1.5059393>
44. Zhuang P, Ng WL, An J, *et al.*, 2019, Layer-by-layer ultraviolet assisted extrusion-based (UAE) bioprinting of hydrogel constructs with high aspect ratio for soft tissue engineering applications. *PLoS One*, 14: e0216776.  
<https://doi.org/10.1371/JOURNAL.PONE.0216776>
45. Li X, Liu B, Pei B, *et al.*, Inkjet bioprinting of biomaterials. *Chem Rev*, 120: 10793–10833.  
[https://doi.org/10.1021/acs.chemrev.0c00008/asset/images/large/cr0C00008\\_0028.JPEG](https://doi.org/10.1021/acs.chemrev.0c00008/asset/images/large/cr0C00008_0028.JPEG)
46. Ng WL, Huang X, Shkolnikov V, *et al.*, 2022, Controlling droplet impact velocity and droplet volume: Key factors to achieving high cell viability in sub-nanoliter droplet-based bioprinting. *Int JBioprint*, 8: 424.  
<https://doi.org/10.18063/IJB.V8I1.424>

47. Li W, Mille LS, Robledo JA, *et al.*, 2020, Recent advances in formulating and processing biomaterial inks for vat polymerization-based 3D printing. *Adv Healthc Mater*, 9: 2000156.  
<https://doi.org/10.1002/ADHM.202000156>
48. Cooley P, Wallace D, Antohe B, 2016, Applications of ink-jet printing technology to BioMEMS and microfluidic systems. *J Assoc Lab Auto*, 7: 33–39.  
<https://doi.org/10.1016/S1535-5535-04-00214-X>
49. Fuller SB, Wilhelm EJ, Jacobson JM, 2002, Ink-jet printed nanoparticle microelectromechanical systems. *J Microelectromech Syst*, 11: 54–60.
50. Hebner TR, Wu CC, Marcy D, *et al.*, 2022, Ink-jet Printing of Doped Polymers for Organic Light Emitting Devices. Available from: <https://www.ojps.aip.org/aplo/aplcr.jsp> [Last accessed on 2022 Mar 27].
51. Wallace D, 2005, Ink-jet Printing as a Tool in Manufacturing and Instrumentation. Nanolithography and Patterning Techniques in Microelectronics. Netherlands: Elsevier. p.267.
52. Perkins J, Hong Y, Ye SH, *et al.*, 2014, Direct writing of bio-functional coatings for cardiovascular applications. *J Biomed Mater Res Part A*, 102: 4290–4300.  
<https://doi.org/10.1002/JBM.A.35105>
53. Perkins J, Xu Z, Smith C, *et al.*, 2015, Direct writing of polymeric coatings on magnesium alloy for tracheal stent applications. *Ann Biomed Eng*, 43: 1158–1165.  
<https://doi.org/10.1007/S10439-014-1169-3/figures/6>
54. Kazemzadeh-Narbat M, Noordin S, Masri BA, *et al.*, 2012, Drug release and bone growth studies of antimicrobial peptide-loaded calcium phosphate coating on titanium. *J Biomed Mater Res Part B Appl Biomater*, 100B: 1344–1352.  
<https://doi.org/10.1002/JBM.B.32701>
55. Le Ray AM, Chiffolleau S, Iooss P, *et al.*, 2003, Vancomycin encapsulation in biodegradable poly( $\epsilon$ -caprolactone) microparticles for bone implantation. Influence of the formulation process on size, drug loading, in vitro release and cytocompatibility. *Biomaterials*, 24: 443–449.  
[https://doi.org/10.1016/S0142-9612\(02\)00357-5](https://doi.org/10.1016/S0142-9612(02)00357-5)
56. Kim HW, Knowles JC, Kim HE, 2005, Hydroxyapatite porous scaffold engineered with biological polymer hybrid coating for antibiotic Vancomycin release. *J Mater Sci Mater Med*, 16: 189–195.  
<https://doi.org/10.1007/S10856-005-6679-Y>
57. De Gans BJ, Duineveld PC, Schubert US, 2004, Inkjet printing of polymers: State of the art and future developments. *Adv Mater*, 16: 203–213.  
<https://doi.org/10.1002/ADMA.200300385>
58. Adameczyk M, Brate EM, Chiappetta EG, *et al.*, 1997, Development of a quantitative vancomycin immunoassay for the Abbott AxSYM analyzer. *Ther Drug Monit*, 19: 571.  
<https://doi.org/10.1097/00007691-199710000-00106>
59. Lawson MC, Bowman CN, Anseth KS, 2007, Vancomycin derivative photopolymerized to titanium kills *S. epidermidis*. *Clin Orthop Rel Res*, 461: 96–105.  
<https://doi.org/10.1097/BLO.0B013E3180986706>
60. Monzón M, Oteiza C, Leiva J, *et al.*, 2001, Synergy of different antibiotic combinations in biofilms of *Staphylococcus epidermidis*. *J Antimicrob Chemother*, 48: 793–801.  
<https://doi.org/10.1093/JAC/48.6.793>
61. Xie Z, Liu X, Jia W, *et al.*, 2009, Treatment of osteomyelitis and repair of bone defect by degradable bioactive borate glass releasing vancomycin. *J Control Rel*, 139: 118–126.  
<https://doi.org/10.1016/J.JCONREL.2009.06.012>
62. Headquarters, AST, 1976, Adhesion Measurement of Thin Films, Thick Films, and Bulk Coatings. Vol. 2. PA: Astm Special Technical Publication. p. 4.
63. ASTM International, 2017, ASTM D3359-17 Standard Test Methods for Rating Adhesion by Tape Test. United States: ASTM International. pp.1–9.
64. Page B, Page M, Noel C, 1993, A new fluorometric assay for cytotoxicity measurements *in vitro*. *Int J Oncol*, 3: 473–476.  
<https://doi.org/10.3892/IJO.3.3.473>
65. Adams CS, Antoci Jr V, Harrison G, *et al.*, 2009, Controlled release of vancomycin from thin sol-gel films on implant surfaces successfully controls osteomyelitis. *J Orthop Res*, 27: 701–709.  
<https://doi.org/10.1016/J.JCONREL.2010.04.002>
66. Li B, Brown KV, Wenke JC, *et al.*, 2010, Sustained release of vancomycin from polyurethane scaffolds inhibits infection of bone wounds in a rat femoral segmental defect model. *J Control Release*, 145: 221–230.  
<https://doi.org/10.1016/J.EJPB.2008.05.020>
67. Ruiz JC, Alvarez-Lorenzo C, Taboada P, *et al.*, 2008, Polypropylene grafted with smart polymers (PNIPAAm/PAAc) for loading and controlled release of vancomycin. *Eur J Pharm Biopharm*, 70: 467–477.  
<https://doi.org/10.1016/J.TCA.2006.04.013>
68. Meejoo S, Maneeprakorn W, Winotai P, 2006, Phase and thermal stability of nanocrystalline hydroxyapatite prepared via microwave heating. *Thermochimica Acta*, 447: 115–120.  
<https://doi.org/10.1016/J.MSEC.2015.09.081>
69. Roy A, Jhunjhunwala S, Bayer E, *et al.*, 2016, Porous calcium phosphate-poly (lactic-co-glycolic) acid composite bone cement: A viable tunable drug delivery system. *Mater Sci Eng C Mater Biol Appl*, 59: 92–101.  
<https://doi.org/10.1016/J.MSEC.2015.09.081>
70. Dorozhkin S v. Amorphous calcium (ortho)phosphates.

- Acta Biomaterialia*. 2010;6(12):4457–4475. doi:10.1016/J.ACTBIO.2010.06.031
71. Habibovic P, Barralet JE, 2011, Bioinorganics and biomaterials: Bone repair. *Acta Biomater*, 7: 3013–3026.  
<https://doi.org/10.1016/J.ACTBIO.2011.03.027>
72. Hoppe A, Güldal NS, Boccaccini AR, 2011, A review of the biological response to ionic dissolution products from bioactive glasses and glass-ceramics. *Biomaterials*, 32: 2757–2774.  
<https://doi.org/10.1016/J.BIOMATERIALS.2011.01.004>
73. Lee SH, Lee JE, Baek WY, *et al.*, 2004, Regional delivery of vancomycin using pluronic F-127 to inhibit methicillin resistant *Staphylococcus aureus* (MRSA) growth in chronic otitis media *in vitro* and *in vivo*. *J Controlled Release*, 96: 1–7.  
<https://doi.org/10.1016/J.JCONREL.2003.12.029>
74. Ginebra MP, Traykova T, Planell JA, 2006, Calcium phosphate cements as bone drug delivery systems: A review. *J Control Release*, 113: 102–110.  
<https://doi.org/10.1016/J.JCONREL.2006.04.007>
75. Edin ML, Miclau T, Lester GE, *et al.*, 1996, Effect of cefazolin and vancomycin on osteoblasts *in vitro*. *Clin Orthop Relat Res*, 333: 245–251.
76. Antoci V Jr., Adams CS, Hickok NJ, *et al.*, 2007, Antibiotics for local delivery systems cause skeletal cell toxicity *in vitro*. *Clin Orthop Rel Res*, 462: 200–206.  
<https://doi.org/10.1097/BLO.0B013E31811FF866>
77. Haleem AA, Rouse MS, Lewallen DG, *et al.*, 2004, Gentamicin and vancomycin do not impair experimental fracture healing. *Clin Orthop Rel Res*, 427: 22–24.  
<https://doi.org/10.1097/01.BLO.0000144477.43661.59>
78. McLaren JS, White LJ, Cox HC, *et al.*, 2014, A biodegradable antibiotic-impregnated scaffold to prevent osteomyelitis in a contaminated *in vivo* bone defect model. *Eur Cells Mater*, 27: 332–349.  
<https://doi.org/10.22203/ECM.V027A24>
79. Mason EO, Lamberth LB, Hammerman WA, *et al.*, 2009, Vancomycin MICs for *Staphylococcus aureus* vary by detection method and have subtly increased in a pediatric population since 2005. *J Clin Microbiol*, 47: 1628–1630.  
<https://doi.org/10.1128/JCM.00407-09>
80. Moise PA, North D, Steenbergen JN, *et al.*, 2009, Susceptibility relationship between vancomycin and daptomycin in *Staphylococcus aureus*: Facts and assumptions. *Lancet Infect Dis*, 9: 617–624.  
[https://doi.org/10.1016/S1473-3099\(09\)70200-2](https://doi.org/10.1016/S1473-3099(09)70200-2)
81. Peña J, Corrales T, Izquierdo-Barba I, *et al.*, 2006, Long term degradation of poly( $\epsilon$ -caprolactone) films in biologically related fluids. *Polym Degradation Stability*, 91: 1424–1432.  
<https://doi.org/10.1016/J.POLYMDEGRADSTAB.2005.10.016>
82. Yeh ML, Chen KH, Chen HD, *et al.*, 2013, Prolonged antibiotic release by PLGA encapsulation on titanium alloy. *J Med Biol Eng*, 2013 33(1): p 5.
83. Kim HW, Lee EJ, Jun IK, *et al.*, 2005, Degradation and drug release of phosphate glass/polycaprolactone biological composites for hard-tissue regeneration. *J Biomed Mater Res Part B Appl Biomater*, 75B: 34–41.  
<https://doi.org/10.1002/JBM.B.30223>
84. Fang T, Wen J, Zhou J, *et al.*, 2012, Poly ( $\epsilon$ -caprolactone) coating delays vancomycin delivery from porous chitosan/ $\beta$ -tricalcium phosphate composites. *J Biomed Mater Res Part B Appl Biomater*, 100B: 1803–1811.  
<https://doi.org/10.1002/JBM.B.32747>
85. Uskokovic V, Desai TA, 2013, Phase composition control of calcium phosphate nanoparticles for tunable drug delivery kinetics and treatment of osteomyelitis. II. Antibacterial and osteoblastic response. *J Biomed Mater Res A*, 101: 1427–1436.  
<https://doi.org/10.1002/JBM.A.34437>
86. Kirkham J, Brookes SJ, Shore RC, *et al.*, 2002, Physico-chemical properties of crystal surfaces in matrix–mineral interactions during mammalian biomineralisation. *Curr Opin Colloid Interface Sci*, 7: 124–132.
87. Dos Santos EA, Farina M, Soares GA, *et al.*, 2008, Surface energy of hydroxyapatite and  $\beta$ -tricalcium phosphate ceramics driving serum protein adsorption and osteoblast adhesion. *J Mater Sci Mater Med*, 19: 2307–2316.  
<https://doi.org/10.1007/S10856-007-3347-4/FIGURES/7>
88. Mueller B, Zacharias M, Rezwani K, 2010, Bovine serum albumin and lysozyme adsorption on calcium phosphate particles. *Adv Eng Mater*, 12: B53–B61.  
<https://doi.org/10.1002/ADEM.200980024>
89. Combes C, Rey C, 2010, Amorphous calcium phosphates: Synthesis, properties and uses in biomaterials. *Acta Biomater*, 6: 3362–3378.  
<https://doi.org/10.1016/J.ACTBIO.2010.02.017>